LSCEC: Design of a High-efficiency Leaf-image Segmentation & Classification Model via Ensemble Compute Processes

Aditya P. Bakshi[1], Dr. Vijaya K. Shandilya[2]
[1]Jawaharlal Darda Institute of Engineering & Technology, Yavatmal(M.S) India.
[2]SIPNA College of Engineering & Technology, Amravati (M.S) India.
Email: bakshi.aditya.ab@gmail.com
DOI: 10.47750/pnr.2022.13.S06.301

Abstract

Real-time leaf image segmentation requires consideration of shadow effects, light variations, capture-angle variations, and zoom effects. Designing an efficient segmentation model that is capable of considering these effects is highly complex, and requires context-specific segmentation techniques. Such techniques are computationally complex, and require larger delays, which limits their applicability for real-time use cases. Moreover, such models are highly context-sensitive and require continuous reconfiguration for multiple image types. To overcome these limitations, this text proposes design of a high-efficiency leaf-image segmentation & classification model via ensemble compute processes. The model initially uses saliency maps for background removal, and cascades it with an ensemble of multiple Fuzzy C Means (FCM) segmentation techniques. These include, Enhanced FCM, k FCM, and original FCM, which results in 3 different image sets. Each of these image sets are individually processed to identify green & yellow coloured foreground pixels. The extracted image mask is filled for better segmentation, and resulting image sets are processed for extraction of features. To efficiently represent the images, a set of Colour, Texture & Convolutional feature maps are extracted, which assists in identification of multidomain feature sets. These feature sets are classified by a combination of Naïve Bayes (NB) Multilayer Perceptron (MLP), Logistic Regression (LR), and Support Vector Machine (SVM) based classification engines, which assists in improving efficiency of disease detection for different crop types. Due to this combination, the proposed model is able to achieve 3.5% better classification accuracy, 1.8% faster response, 4.9% higher precision, and 5.5% better recall when compared with state-of-the-art models. Due to which, the proposed model is capable of deployment for a wide variety of real-time use cases.

Keywords: Segmentation, NB, MLP, SVM, FCM, Saliency.

1. INTRODUCTION

Leaf image segmentation under realistic conditions is a multidomain task that involves background identification, shadow removal, colour variation analysis, image capture angle analysis, and other secondary effects. An efficient segmentation model will assist in improving leaf-classification performance for multiple use cases. A typical classification model [1] is depicted in Fig 1, wherein input leaf images are processed using a 2-step segmentation model that includes binary processing, Laplacian transformations, and morphological operations. These segmentation operations also result in identification of multiple feature sets that are classified via Hidden Naïve Bayes (HNB) classification process. The efficiency of HNB classifier is directly affected by efficiency of the segmentation process. Thus, it is recommended that researchers must deploy highly efficient segmentation models in order to improve their plant-level classification performance levels. A wide variety of Machine Learning based segmentation models are proposed by researchers, which assist in context-independent segmentation operations. These models are highly generic, but have moderate accuracy levels, while context-dependent models are highly complex but need larger computational resources, which limits its scalability levels.

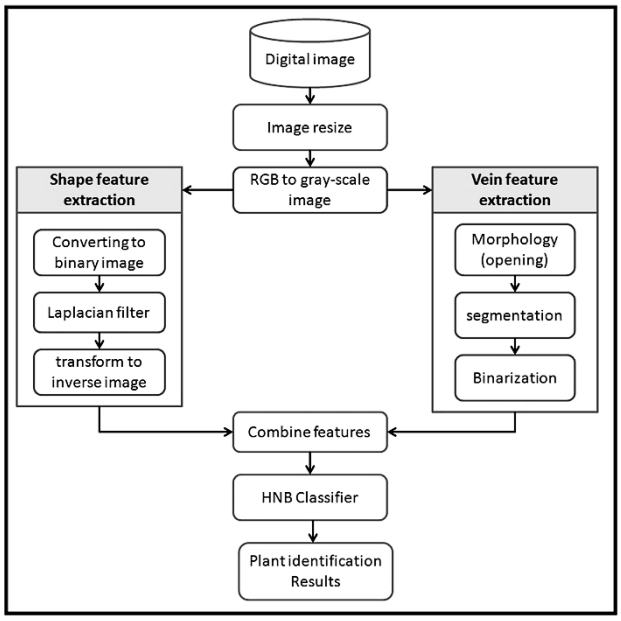

Fig 1. A typical plant-disease classification process

In the following section of this text, we will go over a review of such models [2, 3, 4], discussing their contextual nuances, functional advantages, deployment-specific limitations, and application-specific future scopes. As a result of what has been discussed, it is possible to see that these models are computationally difficult to implement and call for longer delays, which reduces the likelihood that real-time applications can make use of these models. In addition, models of this kind are extremely context-dependent and need constant reconfiguration to accommodate a wide variety of image types. In order to circumvent these restrictions, this article's section 3 makes a suggestion for the design of a high-efficiency leaf-image segmentation and classification model that is accomplished through the use of ensemble compute processes. The efficiency of the proposed model was measured against that of various state-of-the-art models, and its performance was assessed using a variety of image data sets. This piece of writing is brought to a close with some contextual observations regarding the model that has been proposed, as well as some recommendations regarding methods to further optimize its performance levels.

2. Literature Review

Researchers have proposed a wide variety of models for improving classification performance for plant disease sets. For instance, work in [5, 6] proposes use of Lightweight Inception Networks and Feed-Forward Neural Network with Hybrid Metaheuristic Feature Selection (FFNN HMFS) that assists in improving the classification performance for specific disease types. But these models are not scalable, thus cannot be used for large scale deployments. To overcome this issue, work in [7] proposes design of EfficientNetV2, that can be used for multiple plant disease types. Similar models are discussed in [8, 9, 10], which propose use of Deep Convolutional Generative Adversarial Networks (DC GAN), AlexNet, and ensemble Convolutional Neural Networks (eCNN) which enable estimation of high-density features. These features are used to train high efficiency classifiers, that can be deployed for a wide variety of disease types. Extensions to these models are discussed in [11, 12, 13], which propose use of EfficientNetB0 with DenseNet121, Deep Convolutional Neural Networks, and Spatial Pyramid-Oriented Encoder-Decoder Cascade Convolution Neural Network (SPED CCNN), that aims at enhancing feature representation and classification capabilities under on-field deployments.

Models that use high density CNNs [14], Stepwise Transfer Learning [15], Dual Attention with Topology Fusion Generative Adversarial Networks [16], Data Augmentation with Generative Adversarial Networks [17], Deep CNN [18], image compression-based CNN [19], and Restructured Deep Residual Dense Network [20] are also proposed by researchers. These models showcase high-density feature extraction capabilities, but have higher complexity, which reduce their feature representation capabilities. To overcome these issues, work in [21, 22, 23, 24, 25] propose use of DCGAN, Multimodal efficient CNN, fusion of parallel convolution neural network with extreme learning machine (PCNN ELM), ensemble nonlinear support vector machine (EN SVM), and Collaborative Multiple Networks, which aim at enhancing classification efficiency under real-

time image sets. These models are able to showcase low complexity, and high scalability, which makes them useful for multiple disease classification scenarios. Similar models are discussed in [26, 27, 28, 29, 30], which propose use of Deep Neural Method, L1-Norm Minimization Extreme Learning Machine, Deep CNN, Explainable Artificial Intelligence (XAI), and ResNet18 with DenseNet, which allow the model to represent plant images in multiple domains, thereby enhancing their classification performance levels. Extensions to these models are discussed in [31] which propose use of YOLOv4, counting models, Internet of Things (IoT) with machine learning, spectral processing, and Compressed CNN that assist in fine tuning the classification process. But such techniques are computationally complex, and require larger delays, which limits their applicability for real-time use cases. Moreover, such models are highly context-sensitive and require continuous reconfiguration for multiple image types. To overcome these limitations, next section of this text proposes design of a high-efficiency leaf-image segmentation & classification model via ensemble compute processes. The model was validated under multiple use cases to validate its performance for real-time scenarios.

3. Design of the proposed high-efficiency Leaf-image Segmentation & Classification model via Ensemble Compute processes

Based on the review of existing models, it can be observed that are computationally complex, and require larger delays, which limits their applicability for real-time use cases. Moreover, such models are highly context-sensitive and require continuous reconfiguration for multiple image types. To overcome these limitations, this section of the text proposes design of a high-efficiency leaf-image segmentation & classification model via ensemble compute processes. Flow of the model is depicted in Fig 2, where it is observed that the model initially uses saliency maps for background removal, and cascades it with an ensemble of multiple Fuzzy C Means (FCM) segmentation techniques.

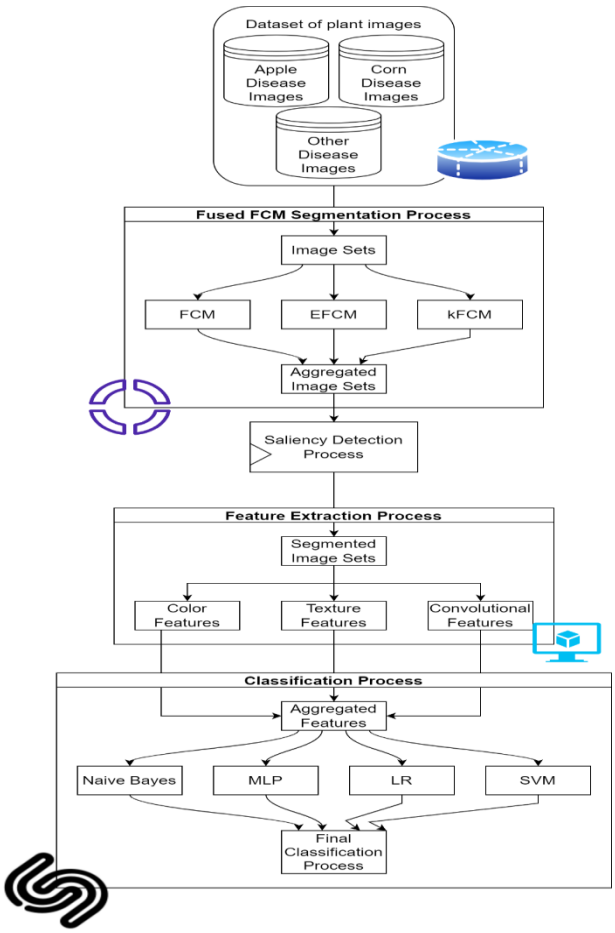

Fig 2. Overall flow of the proposed ensemble FCM, Saliency, Multimodal feature extraction, and ensemble classification process

These include, Enhanced FCM, k FCM, and original FCM, which results in 3 different image sets. Each of these image sets are individually processed to identify green & yellow coloured foreground pixels. The extracted image mask is filled for better segmentation, and resulting image sets are processed for extraction of features. To efficiently represent the images, a set of Colour, Texture & Convolutional feature maps are extracted, which assists in identification of multidomain feature sets. These feature sets are classified by a combination of Naïve Bayes (NB) Multilayer Perceptron (MLP), Logistic Regression (LR), and Support Vector Machine (SVM) based classification engines, which assists in improving efficiency of disease detection for different crop types. The model initially collects different crop leaf images, and segments them via an ensemble of different Fuzzy C Means (FCM) based clustering models. At the core, all these models use a standard FCM process, that works as follows,

To start the clustering process, initialize image size as, x=NM, where N,M represents total rows & columns in the image sets.

Setup constants for FCM such as scaling constant c, a fuzzy constant α, and an error threshold used for completing the cluster formation process $\varepsilon > 0$.

Initialize counter t=0, and stochastically initialize cluster centroids V

Find the distance metric u via equation 1,

$$u = \left[\sum_{i=1}^{C}\left(\frac{d_{ij}}{d_{jk}}\right)^{\frac{2}{\alpha-1}}\right]^{-1} \ldots (1)$$

Where, d is the Euclidean distance, calculated between initial centroids V and the pixels.

Generate new centroids via equation 2,

$$V(New) = \frac{\sum_{i=1}^{\alpha} u^{t+1} * x_i}{\sum_{i=1}^{\alpha} u^{t+1}} \ldots (2)$$

Continue these optimizations equation 3 is not true,

$$V(New) - V < \varepsilon \ldots (3)$$

Once the operations are completed, de-fuzzify centroids via equation 4,

$$c = \arg(max(u)) \ldots (4)$$

Based on this process, all image pixels are clustered into foreground & background pixels. This is done in order to group together all regions leaf pixels. Such images are obtained for EFCM and kFCM as well, and they are post-processed via the following process,

In each cluster with RGB pixels, estimate green-to-red ratio, and green-to-blue ratio at pixel-level via equations 5 and 6,

$$GR = \frac{G}{R} \ldots (5)$$

$$GB = \frac{G}{B} \ldots (6)$$

Count the pixels where GR>1, and GB>1, which indicates green colour is more prevalent than other colours.

Select the cluster where higher count of green pixels is available, and use them for fusion operations.

Images from FCM, EFCM, and kFCM are combined via equation 7,

$$I_{out} = \frac{I(FCM) + I(EFCM) + I(kFCM)}{3} \dots (7)$$

This allows the model to identify leaf regions and remove any unwanted shadow effects, and overlap effects. To further fine tune the segmentation of images, a saliency map is extracted which assists in removing outlier pixels via an entropy estimation process. This process can be observed from Fig 3, and initially extracts bit plane slices from input image via equation 8,

$$S_i = \bigcup_{r,c}^{N,M} \left(P_{r,c} \bigoplus 2^i \right) \dots (8)$$

Where, S_i is the i^{th} slice, and $P_{r,c}$ represents grey level of the pixel, for R, C row sets & column sets. For each of these slices identify intensity levels (Y), chrominance (C_r) and luminance (C_b) levels. These levels are estimated for every slice via equations 9, 10 and 11 as follows,

$$Y = 16 + (65.481 * R + 128.553 * G + 24.966 * B) \dots (9)$$

$$C_b = 128 + (-37.797 * R - 74.203 * G + 112 * B) \dots (10)$$

$$C_r = 128 + (112 * R - 93.786 * G - 18.214 * B) \dots (11)$$

Where, R,G,B represents red, green and blue levels for different image slices.

Once these values are estimated, then calculate approximate energy levels via equation 12,

$$I_a = \frac{1}{N * M} * \sum_{r,c}^{N,M} C_i \dots (12)$$

Where, C_i are pixel intensities for RGB & YC_bC_r colour domains, and I_a represents average image entropy levels. Also, estimate distance between different pixel sets via equation 13,

$$d(s_i, s_j) = \frac{1}{N * M} * \sum_{i=1}^{N_S} I_{avg_i} * \sqrt{\sum_{r,c}^{N,M} \frac{(P_{i_r} - P_{j_r})^2 + (P_{i_c} - P_{j_c})^2}{Var(s_i, s_j)}} \dots (13)$$

Where, $d(s_i, s_j)$ is distance between 2 slices; while $Var(s_i, s_j)$ represents level of variance between these slices, N_s are total slices extracted and P_{x_y} represents pixel intensity levels for x^{th} coloured image in the y^{th} set of dimensions.

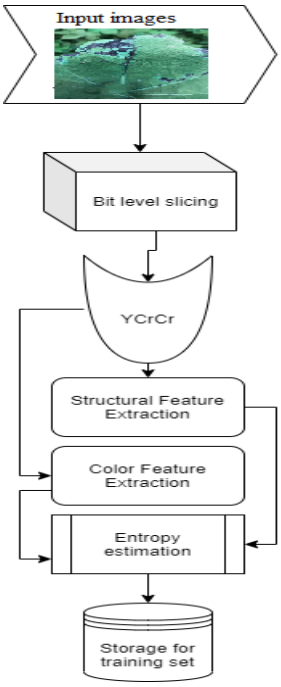

Fig 3. Saliency Map Detection Process

These distance vectors are evaluated for each colour space, and pixels with values more than d are retained, while others are removed to get saliency images. The results of this process can be observed from Fig 4 as follows,

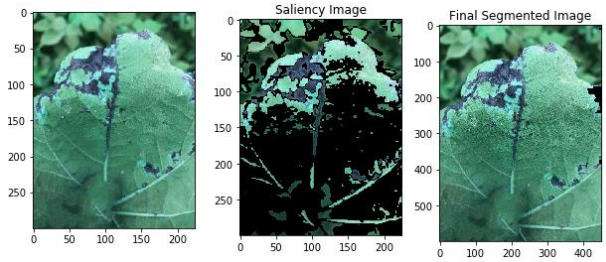

Fig 4. Sample of Saliency Maps for Apple images

To further represent these images, Colour Maps, Edge Maps and Gabor Maps are extracted via the following process,

- To convert extracted images into equalized ranges, they are quantized via equation 14,

$$P_{quant} = {}^{P_{in} * 128}/_{P_{max}} \dots (14)$$

Where, $P_{in}, P_{quant}, and\ P_{max}$ represents input colour pixels, output quantized colour pixels, and maximum intensity of pixels.

- From these quantized pixels, estimate extended histogram colour maps via equation 15,

$$CF_{out} = \bigcup_{i=1}^{N_s} \sum_{r,c}^{N,M} \left| P_{r,c} == P_{quant_{r,c}} \right| \dots (15)$$

Where, CF_{out} represents output colour features, while N_s represents total number of saliency pixels. Also calculate shape features using Canny edge detection via equation 16,

$$SF_{out} = \bigcup_{i=1}^{N_S} \sum_{r,c}^{N,M} \left| Canny\left(P_{r,c}, P_{r,c+1}\right) == 1 \right| \dots (16)$$

Where, SF_{out} represents shape feature sets, $Canny(P_{r,c})$ represents the edge detected image pixels via Canny detection process. Now estimate coarse entropy levels from these features via equation 17,

$$E_{f_i} = -\sum_{r=1}^{N}\sum_{c=1}^{M} p\left(F_{r,c_i}\right) * \log\left(p\left(F_{r,c_i}\right)\right) \dots (17)$$

Where, $p\left(F_{r,c_i}\right)$ are the pixels that have intensities more than average pixels levels. These pixel sets are used to estimate colour maps, edge maps and Gabor feature maps via equations 18, 19 and 20 as follows,

$$CMap_s = \bigcup_{c=1}^{255} \sum_{i=1}^{R} \sum_{j=1}^{C} \sum_{a=1}^{Colors} \left(I_{i,j,a_s} == c\right) \dots (18)$$

$$Edge_s = \sum_{i=1}^{R}\sum_{j=1}^{C} \frac{\sum_{a=1}^{Colors} P\left(E(I_{i,j,a_s})\right)}{R * C * a} \dots (19)$$

$$G(x,y)_s = e^{\frac{-x`^2 + \partial^2 * y'^2}{2 * \emptyset^2}} * \cos\left(2 * \frac{pi}{\lambda} * x'\right) \dots (20)$$

Where, $E, \lambda, \partial, \& \emptyset$ represents edge level pixels, Gabor wavelet levels, Gabor scaling levels, and Gabor angular components. These features are combined with convolutional features in order to represent input image sets in terms of windowed components. These features are extracted via equation 21 as follows,

$$Conv_{s_{i,j}} = \sum_{a=-\frac{m}{2}}^{\frac{m}{2}} \sum_{b=-\frac{n}{2}}^{\frac{n}{2}} I_s(i-a, j-b) * ReLU\left(\frac{m}{2} + a, \frac{n}{2} + b\right) \dots (21)$$

Where, m, n are rows & columns of windows, I_s & $ReLU$ are saliency image sets & rectilinear unit for feature activations, while a, b are rows & column sizes for strides. These features are aggregated in order to form a Super Feature Vector (SFV), which is used to categorize the leaf images into different disease types. For this purpose, a combination of Naïve Bayes (NB), Multilayer Perceptron (MLP), Linear Regression (LR), and Support Vector Machine (SVM) based classifiers. These classifiers along with their internal configurations are selected as follows,

- Naïve Bayes
  - Priors = Variance of selected features
  - Smoothing Value $SV = \frac{Var(F)}{Mean(F)} \dots (22)$

Where, Var & $Mean$ are the variance levels, and mean values of selected features

- Multilayer Perceptron
  - Number of hidden layers = $N_{classes}$
  - Activation function = Rectilinear Unit
  - Solver Type = Adam
  - Learning Rate = 0.5
- Logistic Regression

- Tolerance = 0.001
- Class Weights = Class-based variance levels
- Solver Type = Linear
- Maximum Iterations = $10 * N_{feat}$

- Support Vector Machine
- Error Tolerance = 0.0001
- Kernel Type = Radial Basis Function
- Class Weights = Class-based variance levels

Based on these parameters, input images are classified into different disease classes. Results of these classifiers are combined via equation 23 as follows,

$$c_{out} = A(NB) * c_{out}(NB) + A(MLP) * c_{out}(MLP) + A(SVM) * c_{out}(SVM) + A(LR) * c_{out}(LR) \dots (23)$$

Where, A & c_{out} represents accuracy levels and output classes for different classes. The classifier is used to categorize input images into Apple disease, Cotton Disease, Corn Disease, and Healthy images. Performance of the model was validated on different datasets, and compared with various state-of-the-art models in the next section of this text.

4. Result analysis & comparison

The proposed model uses a combination of multimodal FCM-based segmentation and Saliency Maps to extract regions of interest, which are then represented as high-density feature sets via multiple feature extraction layers. Using an ensemble classification layer, these image sets are classified with high efficiency into Apple diseases, Cotton diseases, Corn diseases, and Healthy image sets. This model's performance was evaluated based on classification accuracy (A), precision (P), recall (R), and classification delay for crop samples obtained from the following sources,

- Plant Village Dataset from Kaggle, which can be downloaded from https://www.kaggle.com/datasets/emmarex/plantdisease

- New Plant Diseases Dataset, which is available at https://www.kaggle.com/datasets/vipoooool/new-plant-diseases-dataset

The model was compared with FFNN HMFS [6], DC GAN [8], and SPED CCNN [13], which are recently proposed classification models, and showcase high performance levels. The accuracy, precision, recall & delay were evaluated via equations 24, 25, 26 & 27 as follows,

$$A = \frac{t_p + t_n}{t_p + t_n + f_p + f_n} \dots (24)$$

$$P = \frac{t_p}{t_p + f_p} \dots (25)$$

$$R = \frac{t_p}{t_p + t_n + f_p + f_n} \dots (26)$$

$$d = \frac{1}{N}\sum_{i=1}^{N} t_{end_i} - t_{start_i} \dots (27)$$

Where, t_p, f_p, t_n & f_n represents the true positive (correctly classified into correct class), false positive (incorrectly classified into correct class), true negative (correctly classified into incorrect class), false negative (incorrectly classified into incorrect class), while t_{end} & t_{start} represents the time instances for finishing and starting the classification process. For assessment, a total of 25.000 samples were employed, of which 60% were used for training, 20% for testing, and 20% for validation operations. On the basis of this technique, accuracy was assessed in table 1, where it was contrasted relative to other strategies w.r.t. the number of Evaluation Images (NEI),

Table 1. Accuracy of crop disease classification operations

NEI	A (%) FFNN HMFS [6]	A (%) DC GAN [8]	A (%) SPED CCNN [13]	A (%) This Work
1108	83.16	89.12	90.88	98.79
2225	83.22	89.44	91.08	98.87
3333	83.27	89.74	91.27	98.95
4442	83.32	90.06	91.47	99.02
5558	83.37	90.39	91.66	99.08
6667	83.42	90.72	91.86	99.13
7775	83.48	91.06	92.06	99.17
8892	83.53	91.40	92.28	99.21
10000	83.58	91.73	92.50	99.25
11108	83.63	92.06	92.71	99.29
12225	83.69	92.38	92.93	99.33
13892	83.74	92.71	93.14	99.38
16667	83.79	93.03	93.34	99.44
18058	83.85	93.36	93.55	99.50
19442	83.90	93.68	93.75	99.57
22225	83.95	94.01	93.95	99.63
23608	84.01	94.33	94.16	99.68
25000	84.06	94.66	94.36	99.73

This evaluation and Fig 5 show that the proposed model's use of multiple efficient classification models allows it to demonstrate 14.5% higher accuracy than FFNN HMFS [6], 5.9% higher accuracy than DC GAN [8], and 6.1% higher accuracy than SPED CCNN [13].

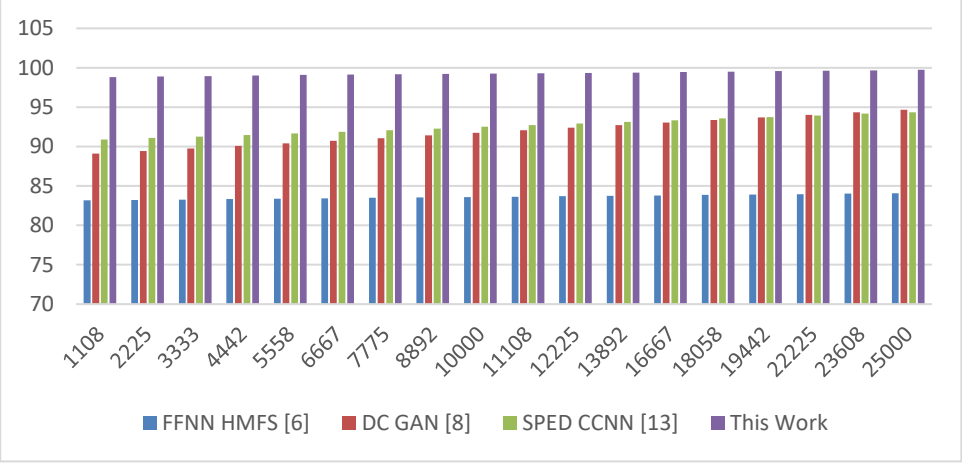

Fig 5. Accuracy of crop disease classification operations

Optimizing its classification performance across multiple disease types was also aided by the incorporation of multimodal feature sets with a high efficiency segmentation layer. The following evaluation in terms of accuracy can be seen in table 2,

Table 2. Precision of crop disease classification operations

NEI	P (%) FFNN HMFS [6]	P (%) DC GAN [8]	P (%) SPED CCNN [13]	P (%) This Work
1108	81.21	85.32	87.88	97.69
2225	81.26	85.63	88.07	97.76
3333	81.31	85.93	88.26	97.82
4442	81.36	86.25	88.45	97.87
5558	81.42	86.56	88.64	97.92
6667	81.47	86.89	88.84	97.96
7775	81.52	87.21	89.04	98.00
8892	81.57	87.52	89.25	98.04
10000	81.63	87.84	89.46	98.08
11108	81.68	88.14	89.66	98.13
12225	81.73	88.45	89.86	98.18
13892	81.78	88.76	90.06	98.24
16667	81.83	89.07	90.25	98.30
18058	81.88	89.37	90.45	98.36
19442	81.93	89.68	90.64	98.42
22225	81.98	89.99	90.83	98.47
23608	82.03	90.30	91.03	98.52

Fig 6 illustrates the results of this evaluation, showing that the proposed model outperforms the state-of-the-art baselines by 16.2%, 8.5%, and 5.9%, respectively.

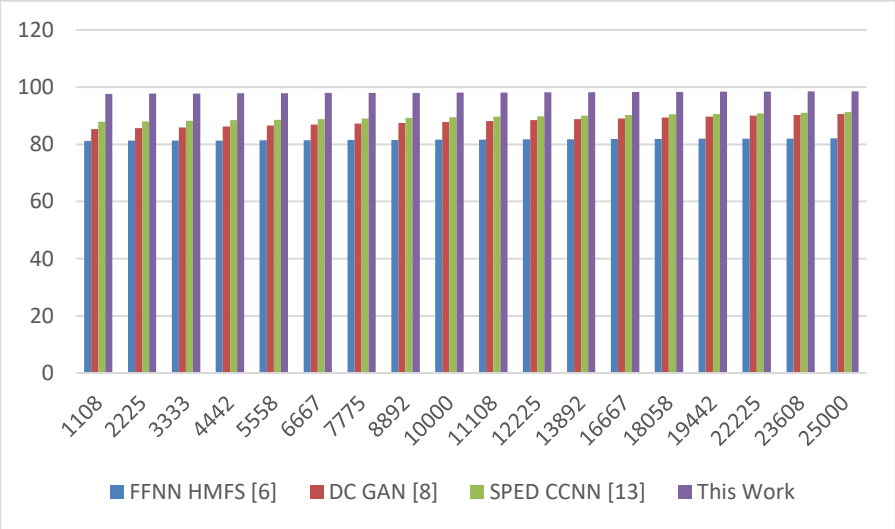

Fig 6. Precision of crop disease classification operations

This improvement is attributable to the model's use of high efficiency feature representation and multiple efficient classification models. Optimizing its classification performance across multiple disease types was also aided by the incorporation of multimodal feature sets with a high efficiency segmentation layer. For quantization purposes, a similar estimation of the number of evaluation images is performed, as shown in table 3, which can be observed below,

Table 3. Recall of crop disease classification operations

NEI	R (%) FFNN HMFS [6]	R (%) DC GAN [8]	R (%) SPED CCNN [13]	R (%) This Work
1108	80.20	87.37	88.37	97.06
2225	80.25	87.68	88.56	97.13
3333	80.30	87.99	88.75	97.20
4442	80.36	88.31	88.95	97.26
5558	80.41	88.64	89.14	97.31
6667	80.46	88.97	89.34	97.35
7775	80.52	89.27	89.53	97.40
8892	80.60	89.53	89.73	97.46
10000	80.69	89.77	89.92	97.52
11108	80.79	89.99	90.10	97.59
12225	80.88	90.22	90.28	97.67
13892	80.96	90.47	90.46	97.74
16667	81.05	90.72	90.64	97.82
18058	81.13	90.96	90.82	97.90
19442	81.21	91.22	91.01	97.98
22225	81.28	91.50	91.19	98.04
23608	81.34	91.80	91.38	98.10
25000	81.40	92.10	91.58	98.16

According to the results of the evaluation presented in Fig 7, the proposed model boasts a 14.5% increase in recall compared to FFNN HMFS [6], a 5.9% increase compared to DC GAN [8], and a 5.5% increase compared to SPED CCNN [13]; this improvement is largely attributable to the model's use of high-efficiency feature representation and segmentation models. Integration of multimodal feature sets with high efficiency segmentation layer helped optimize its classification performance across multiple disease types, contributing to this performance improvement.

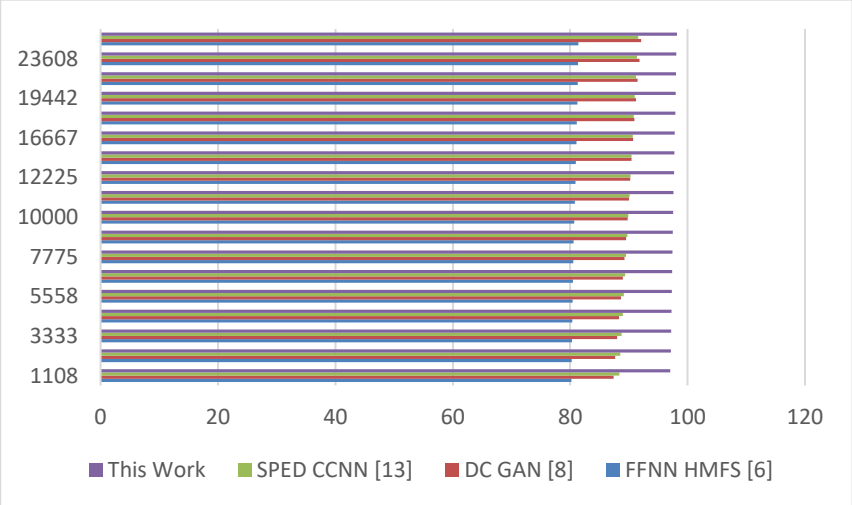

Fig 7. Recall of crop disease classification operations

Table 4 provides a similarly comprehensive evaluation in terms of classification delay levels,

Table 4. Delay of crop disease classification operations

NEI	D (ms) FFNN HMFS [6]	D (ms) DC GAN [8]	D (ms) SPED CCNN [13]	D (ms) This Work
1108	114.13	104.72	106.86	104.84
2225	114.20	105.09	107.09	104.92
3333	114.28	105.47	107.32	104.99
4442	114.35	105.85	107.55	105.06
5558	114.42	106.24	107.78	105.11
6667	114.50	106.63	108.02	105.16
7775	114.57	107.03	108.26	105.20
8892	114.64	107.42	108.51	105.24
10000	114.71	107.81	108.76	105.28
11108	114.79	108.19	109.01	105.33
12225	114.86	108.57	109.26	105.38
13892	114.93	108.95	109.50	105.44
16667	115.01	109.33	109.74	105.50
18058	115.08	109.70	109.98	105.57
19442	115.15	110.08	110.22	105.64
22225	115.23	110.47	110.46	105.69
23608	115.30	110.85	110.70	105.75
25000	115.37	111.24	110.93	105.80

This evaluation and Fig 8 show that the proposed model is able to demonstrate 3.5% lower delay than FFNN HMFS [6], 1.4% lower delay than DC GAN [8], and 1.5% lower delay than SPED CCNN [13], primarily as a result of the deployment of more advanced techniques for feature extraction and classification. Integration of multimodal feature sets with high efficiency segmentation layer helped optimize its classification performance across multiple disease types, contributing to this performance improvement. As a result, the proposed model has the potential for highly efficient disease estimation and numerous real-time applications.

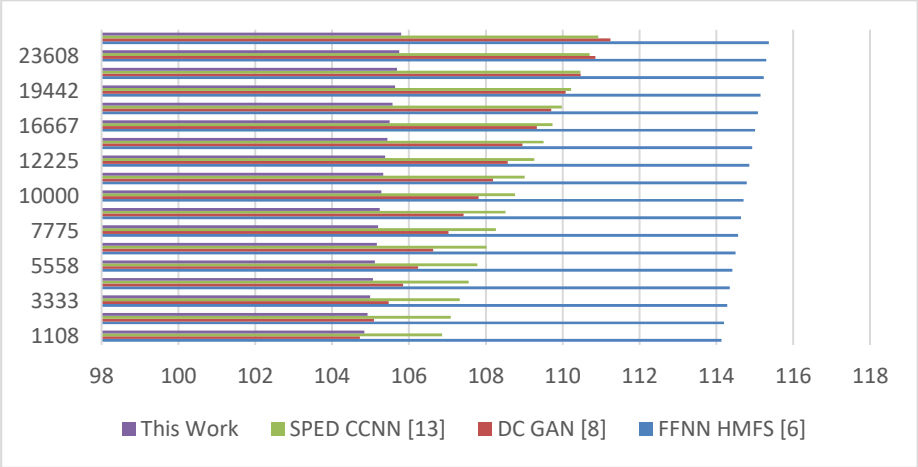

Fig 8. Delay of crop disease classification operations

5. Conclusion and future scope

The proposed model uses a combination of multiple FCM based segmentation with high density feature extraction & ensemble classification operations. These operations assist in improving the classification performance under 4 different plant disease classes, which includes Apple diseases, Cotton diseases, Corn diseases, and Healthy plant images. The proposed method's superior accuracy compared to FFNN HMFS [6], DC GAN [8], and SPED CCNN [13] is largely attributable to the fact that it employs a combination of efficient classification models, each of which contributes to the overall improvement. Integration of multimodal feature sets with high efficiency segmentation layer helped optimize its classification performance across multiple disease types, contributing to this performance improvement. Using high-efficiency feature representation and multiple efficient classification models, the proposed model was able to demonstrate 16.2% higher precision than FFNN HMFS [6], 8.5% higher precision than DC GAN [8], and 5.9% higher precision than SPED CCNN [13]. Integration of multimodal feature sets with high efficiency segmentation layer helped optimize its classification performance across multiple disease types, contributing to this performance improvement. The proposed model also outperformed the three state-of-the-art reference models, FFNN HMFS [6], DC GAN [8], and SPED CCNN [13], with an increase in recall of 14.5%, 5.9%, and 5.5%, respectively, thanks to the incorporation of high-efficiency feature representation and segmentation models. Integration of multimodal feature sets with high efficiency segmentation layer helped optimize its classification performance across multiple disease types, contributing to this performance improvement. With improved feature extraction and classification models, the proposed model achieved a 3.5% reduction in delay compared to FFNN HMFS [6], 1.4% reduction compared to DC GAN [8], and 1.5% reduction compared to SPED CCNN [13] in terms of classification speed. Integration of multimodal feature sets with high efficiency segmentation layer helped optimize its classification performance across multiple disease types, contributing to this performance improvement. As a result, the proposed model has the potential for highly efficient disease estimation and numerous real-time applications. In future, the proposed model's performance can be optimized via integration of hybrid bioinspired techniques which will assist in improving feature selection operations. The model must be validated on larger datasets, and can integrate Autoencoders, and Q-Learning for continuous optimizations under real-time deployments.

REFERENCES

1. Q. H. Cap, H. Uga, S. Kagiwada and H. Iyatomi, "LeafGAN: An Effective Data Augmentation Method for Practical Plant Disease Diagnosis," in IEEE Transactions on Automation Science and Engineering, vol. 19, no. 2, pp. 1258-1267, April 2022, doi: 10.1109/TASE.2020.3041499.
2. X. Liu, W. Min, S. Mei, L. Wang and S. Jiang, "Plant Disease Recognition: A Large-Scale Benchmark Dataset and a Visual Region and Loss Reweighting Approach," in IEEE Transactions on Image Processing, vol. 30, pp. 2003-2015, 2021, doi: 10.1109/TIP.2021.3049334.
3. Y. Zhao et al., "Plant Disease Detection Using Generated Leaves Based on DoubleGAN," in IEEE/ACM Transactions on Computational Biology and Bioinformatics, vol. 19, no. 3, pp. 1817-1826, 1 May-June 2022, doi: 10.1109/TCBB.2021.3056683.
4. G. Delnevo, R. Girau, C. Ceccarini and C. Prandi, "A Deep Learning and Social IoT Approach for Plants Disease Prediction Toward a Sustainable Agriculture," in IEEE Internet of Things Journal, vol. 9, no. 10, pp. 7243-7250, 15 May15, 2022, doi: 10.1109/JIOT.2021.3097379.
5. J. Chen, W. Chen, A. Zeb, S. Yang and D. Zhang, "Lightweight Inception Networks for the Recognition and Detection of Rice Plant Diseases," in IEEE Sensors Journal, vol. 22, no. 14, pp. 14628-14638, 15 July15, 2022, doi: 10.1109/JSEN.2022.3182304.
6. T. N. Pham, L. V. Tran and S. V. T. Dao, "Early Disease Classification of Mango Leaves Using Feed-Forward Neural Network and Hybrid Metaheuristic Feature Selection," in IEEE Access, vol. 8, pp. 189960-189973, 2020, doi: 10.1109/ACCESS.2020.3031914.
7. S. C. K., J. C. D. and N. Patil, "Cardamom Plant Disease Detection Approach Using EfficientNetV2," in IEEE Access, vol. 10, pp. 789-804, 2022, doi: 10.1109/ACCESS.2021.3138920.
8. Q. Zeng, X. Ma, B. Cheng, E. Zhou and W. Pang, "GANs-Based Data Augmentation for Citrus Disease Severity Detection Using Deep Learning," in IEEE Access, vol. 8, pp. 172882-172891, 2020, doi: 10.1109/ACCESS.2020.3025196.
9. M. Lv, G. Zhou, M. He, A. Chen, W. Zhang and Y. Hu, "Maize Leaf Disease Identification Based on Feature Enhancement and DMS-Robust Alexnet," in IEEE Access, vol. 8, pp. 57952-57966, 2020, doi: 10.1109/ACCESS.2020.2982443.
10. S. Barburiceanu, S. Meza, B. Orza, R. Malutan and R. Terebes, "Convolutional Neural Networks for Texture Feature Extraction. Applications to Leaf Disease Classification in Precision Agriculture," in IEEE Access, vol. 9, pp. 160085-160103, 2021, doi: 10.1109/ACCESS.2021.3131002.
11. H. Amin, A. Darwish, A. E. Hassanien and M. Soliman, "End-to-End Deep Learning Model for Corn Leaf Disease Classification," in IEEE Access, vol. 10, pp. 31103-31115, 2022, doi: 10.1109/ACCESS.2022.3159678.
12. E. C. Tetila et al., "Automatic Recognition of Soybean Leaf Diseases Using UAV Images and Deep Convolutional Neural Networks," in IEEE Geoscience and Remote Sensing Letters, vol. 17, no. 5, pp. 903-907, May 2020, doi: 10.1109/LGRS.2019.2932385.
13. Y. Yuan, Z. Xu and G. Lu, "SPEDCCNN: Spatial Pyramid-Oriented Encoder-Decoder Cascade Convolution Neural Network for Crop Disease Leaf Segmentation," in IEEE Access, vol. 9, pp. 14849-14866, 2021, doi: 10.1109/ACCESS.2021.3052769.
14. Y. Wu, X. Feng and G. Chen, "Plant Leaf Diseases Fine-Grained Categorization Using Convolutional Neural Networks," in IEEE Access, vol. 10, pp. 41087-41096, 2022, doi: 10.1109/ACCESS.2022.3167513.
15. M. Ahmad, M. Abdullah, H. Moon and D. Han, "Plant Disease Detection in Imbalanced Datasets Using Efficient Convolutional Neural Networks With Stepwise Transfer Learning," in IEEE Access, vol. 9, pp. 140565-140580, 2021, doi: 10.1109/ACCESS.2021.3119655.
16. Q. Dai, X. Cheng, Y. Qiao and Y. Zhang, "Crop Leaf Disease Image Super-Resolution and Identification With Dual Attention and Topology Fusion Generative Adversarial Network," in IEEE Access, vol. 8, pp. 55724-55735, 2020, doi: 10.1109/ACCESS.2020.2982055.
17. B. Liu, C. Tan, S. Li, J. He and H. Wang, "A Data Augmentation Method Based on Generative Adversarial Networks for Grape Leaf Disease Identification," in IEEE Access, vol. 8, pp. 102188-102198, 2020, doi: 10.1109/ACCESS.2020.2998839.
18. V. Udutalapally, S. P. Mohanty, V. Pallagani and V. Khandelwal, "sCrop: A Novel Device for Sustainable Automatic Disease Prediction, Crop Selection,

and Irrigation in Internet-of-Agro-Things for Smart Agriculture," in IEEE Sensors Journal, vol. 21, no. 16, pp. 17525-17538, 15 Aug.15, 2021, doi: 10.1109/JSEN.2020.3032438.
19. S. Nesteruk et al., "Image Compression and Plants Classification Using Machine Learning in Controlled-Environment Agriculture: Antarctic Station Use Case," in IEEE Sensors Journal, vol. 21, no. 16, pp. 17564-17572, 15 Aug.15, 2021, doi: 10.1109/JSEN.2021.3050084.
20. C. Zhou, S. Zhou, J. Xing and J. Song, "Tomato Leaf Disease Identification by Restructured Deep Residual Dense Network," in IEEE Access, vol. 9, pp. 28822-28831, 2021, doi: 10.1109/ACCESS.2021.3058947.
21. Q. Wu, Y. Chen and J. Meng, "DCGAN-Based Data Augmentation for Tomato Leaf Disease Identification," in IEEE Access, vol. 8, pp. 98716-98728, 2020, doi: 10.1109/ACCESS.2020.2997001.
22. R. R. Patil and S. Kumar, "Rice-Fusion: A Multimodality Data Fusion Framework for Rice Disease Diagnosis," in IEEE Access, vol. 10, pp. 5207-5222, 2022, doi: 10.1109/ACCESS.2022.3140815.
23. S. Huang, G. Zhou, M. He, A. Chen, W. Zhang and Y. Hu, "Detection of Peach Disease Image Based on Asymptotic Non-Local Means and PCNN-IPELM," in IEEE Access, vol. 8, pp. 136421-136433, 2020, doi: 10.1109/ACCESS.2020.3011685.
24. G. Nagasubramanian, R. K. Sakthivel, R. Patan, M. Sankayya, M. Daneshmand and A. H. Gandomi, "Ensemble Classification and IoT-Based Pattern Recognition for Crop Disease Monitoring System," in IEEE Internet of Things Journal, vol. 8, no. 16, pp. 12847-12854, 15 Aug.15, 2021, doi: 10.1109/JIOT.2021.3072908.
25. G. Yang, G. Chen, Y. He, Z. Yan, Y. Guo and J. Ding, "Self-Supervised Collaborative Multi-Network for Fine-Grained Visual Categorization of Tomato Diseases," in IEEE Access, vol. 8, pp. 211912-211923, 2020, doi: 10.1109/ACCESS.2020.3039345.
26. S. Ahmed, M. B. Hasan, T. Ahmed, M. R. K. Sony and M. H. Kabir, "Less is More: Lighter and Faster Deep Neural Architecture for Tomato Leaf Disease Classification," in IEEE Access, vol. 10, pp. 68868-68884, 2022, doi: 10.1109/ACCESS.2022.3187203.
27. R. Dwivedi, T. Dutta and Y. -C. Hu, "A Leaf Disease Detection Mechanism Based on L1-Norm Minimization Extreme Learning Machine," in IEEE Geoscience and Remote Sensing Letters, vol. 19, pp. 1-5, 2022, Art no. 8019905, doi: 10.1109/LGRS.2021.3110287.
28. S. M. Hassan and A. K. Maji, "Plant Disease Identification Using a Novel Convolutional Neural Network," in IEEE Access, vol. 10, pp. 5390-5401, 2022, doi: 10.1109/ACCESS.2022.3141371.
29. Z. Zinonos, S. Gkelios, A. F. Khalifeh, D. G. Hadjimitsis, Y. S. Boutalis and S. A. Chatzichristofis, "Grape Leaf Diseases Identification System Using Convolutional Neural Networks and LoRa Technology," in IEEE Access, vol. 10, pp. 122-133, 2022, doi: 10.1109/ACCESS.2021.3138050.
30. R. Zhang, J. You and J. Lee, "Detecting Pine Trees Damaged by Wilt Disease Using Deep Learning Techniques Applied to Multi-Spectral Images," in IEEE Access, vol. 10, pp. 39108-39118, 2022, doi: 10.1109/ACCESS.2022.3155531.
31. F. Li et al., "A Remote Sensing and Airborne Edge-Computing Based Detection System for Pine Wilt Disease," in IEEE Access, vol. 9, pp. 66346-66360, 2021, doi: 10.1109/ACCESS.2021.3073929.